09

Luminescence tomography of upconversion luminophores with discrete distribution

© L.A. Nurtdinova,[1] A.V. Leontyev,[1] E.O. Mityushkin,[1] D.A. Bizyaev,[1] N.I. Nurgazizov,[1] A.P. Chuklanov,[1] P.A. Kosach,[2] D.G. Zverev,[2] V.G. Nikiforov[1]

[1]Federal Research Center „Kazan Scientific Center of Russian Academy of Sciences“,
420029 Kazan, Russia
[2]Kazan Federal University,
420008 Kazan, Russia
e-mail: niazn@mail.ru

Received April 21, 2025
Revised April 21, 2025
Accepted April 21, 2025

Test measurements of a discrete structure model were performed using confocal optical microscopy and luminescence tomography techniques. This test structure, which has a pronounced discrete distribution of upconversion phosphoraggregates, was created using atomic force microscopy techniques. Particles of the chosen luminophore $NaYF_4$:Yb(18 %), Er(2 %), were synthesized using the hydrothermal method. Their upconversion luminescence in the visible spectrum upon near-infrared laser excitation at around 980 nm makes them attractive for a wide range of bioimaging applications. Using confocal microscopy, the luminescent signal was recorded with 3D spatial resolution. The comparative analysis of post-processing algorithms applied to experimental data showed that, in the case of a pronounced discrete distribution of luminophores, accounting for the point spread function in deconvolution processing allows both to level image artifacts and to significantly increase the accuracy of determining the size of luminescent objects.

Keywords: confocal microscopy, image deconvolution, fluorescence tomography, atomic force microscopy, upconversion luminophores, fluoride particles.

DOI: 10.61011/TP.2025.10.62075.67-25

Introduction

Visualization of cellular and subcellular structures within a biological tissue is becoming one of the fundamental research, diagnosis and therapy techniques in biomedicine. Development of techniques for visualization of objects under the surface, deep in the sample is the essential area of research. For this purpose, high-resolution tomography techniques such as optical coherence tomography [1], confocal microscopy [2], chromatic confocal microscopy [3], etc. have been developed.

The most widely available confocal optical microscopy (COM) technique is used to detect radiation from a sample area less than $1\,\mu m^2$. Upconversion nanoprobes are promising devices for biological applications They can absorb radiation in the transparency region of biological tissues, i.e. in the near IR range, and emit visible light. Upconversion nanoprobes are widely used for visualization of various processes (for example, drug transport), which also enables imaging using confocal optical microscopy methods [4–9]. Due to the specific features of nanoprobe distribution in biotissues, highly nonuniform or even distinctly discrete distribution of luminescent probes over the volume should be expected. Note that a traditional confocal microscope mode, in which radiation reflected from a surface is detected, is in the vast majority of cases used when the a signal source is spatially continuous. However, signal detection in media with discrete luminophore distribution may be accompanied by appearance of artefacts that will strongly distort their real layout. This determines the strong need for evaluating the artefact size and for development of artefact minimization and total removal methods.

Media with unknown luminescent probe distribution (for example, biotissues) are unsuitable for meeting the assigned tasks. A sample with an a-priori known accurate layout of luminescent objects with predefined properties and capability to vary object sizes and positions is required for the experiment. This sample may be prepared using atomic force microscopy methods to characterize and handle nanoobjects with a nanometer accuracy. This work proposes a technique for fabrication a test structure on the basis of upconversion $NaYF_4$:Yb, Er particles capable of emitting visible bright light when exposed to laser excitation at a wavelength near 980 nm. Tomography of such structure was performed using confocal microscopy methods and accuracy of the obtained data on positions and sizes of luminescent objects was evaluated.

1. Preparation of samples and measurement procedure

1.1. Upconversion particle synthesis $NaYF_4$:Yb(18 %), Er(2 %)

Synthesis of $NaYF_4$:Yb(18 %), Er(2 %) particles was performed by a hydrothermal method that is described in

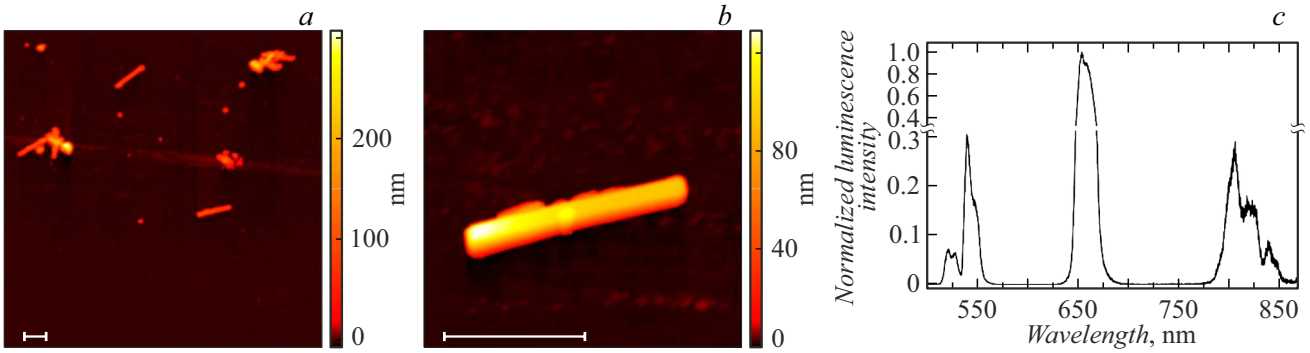

Figure 1. AFM image of a glass substrate with deposited $NaYF_4$:Yb, Er particles (a) and magnified AFM image of a single particle (b). Scale bar size is 1 μm. Upconversion luminescence spectra of particles exposed to laser excitation at 980 nm (c).

detail, for example, in [10–12]. According to the obtained AFM images (Figure 1, a, b), the synthesized particles had a cylindrical shape with typical dimensions of approximately $1 \times 0.12\,\mu$m. The luminescence spectrum measured using COM (Figure 1, c) corresponds to upconversion emission of Er^{3+} under 974 nm laser excitation [11,12].

1.2. Atomic-force microscope

A test structure on the substrate surface was formed and characterized using the Solver Bio scanning probe microscope (SPM) (NT-MDT, Russia) operated in the atomic-force microscope (AFM) mode. Due to a probe movement scheme used to scan a sample, SPM was equipped with the Biolam P2-1 inverted optical microscope placed on the substrate back side with respect to the sensing head. Therefore, when using transparent substrates, a sampling region could be found repeatedly (using scratch marks) and the AFM probe could be positioned above the sampling area with an error lower than 5 μm for formation and investigation of the test structure. An available AFM scanning field was about $100 \times 100\,\mu$m, and further accurate positioning of the AFM probe could be performed by the SPM control program. The optical microscope was also used to control AFM probe movements during scanning and, if required, to adjust the size of scanning region and its position within the maximum scanning field.

Tap150Al-G standard silicon probes (Budgetsensors), resonance frequency about 150 kHz, force constant about 5 N/m, were used. These probes may be used in a contact mode, where the force of interaction with the surface is sufficiently high to move particles, and also in a semi-contact mode, where the interaction force is lower by several orders of magnitude, and, thus allowing the examination of the obtained structures. The test structure was formed and examined at room temperature and humidity.

1.3. Confocal optical microscope

The main COM system components are objectives, pinhole, light detectors, scanning mirrors (galvanometer scanner), beam splitters set to excitation laser and luminescent signal wavelengths [13,14], and a spectrometer. CM96Z200-74 series single-mode laser diode with a fiber Bragg grating (II−VI Incorporated) with a central wavelength of 974 nm falling within the Yb^{3+} absorption band was used as an excitation source. Olympus PlanN 10x/0.25 objective was used to focus light on the object and collect light from the object. Maximum lateral resolution of the microscope was determined by the excitation spot diameter in the focal plane and was equal to 1.1 μm. Radiation was detected in photon counting mode using the PelkinElmer STCM-AQR-14-FC silicon avalanche photodiode. The collected signal was visualized and analyzed in Qudi [15]. Luminescence spectrum corresponded to Er^{3+} radiation lines excited through Yb^{3+} according to an upconversion scheme [11,12]. Luminescence spectra were recorded using the Starlight Xpress Trius SX-694 CCD-camera spectrometer.

1.4. Fabrication of a sample with controlled discrete distribution of luminescent regions

A 0.45 mm cover glass was used as a substrate for formation of the test structure. An irregularly shaped piece with dimensions of about 2×0.4 cm was cut from the glass and had a bevel for quick identification of the working side of the substrate. Then, marks in the form of microscratches intersecting each other at $\sim 90°$ were formed on the surface. The resulting microscratch intersections were easily visually identified to quickly find the desired region on the substrate when creating and investigating the physical properties of the test structure using various methods [16].

The test structure was formed using a previously proposed AFM particle imprinting algorithm [17] improved for more precise manipulations. A drop of solution with upconversion particles was applied onto substrate № 1. Then, using the optical microscope, a region that assuredly contained many particles was chosen near the microscratch intersection. The AFM probe set to the semi-contact mode was brought to this region to scan a $90 \times 90\,\mu$m surface area. During optical microscope scanning, probe movements and behavior of the film with upconversion particles were controlled. Analysis of the recorded AFM

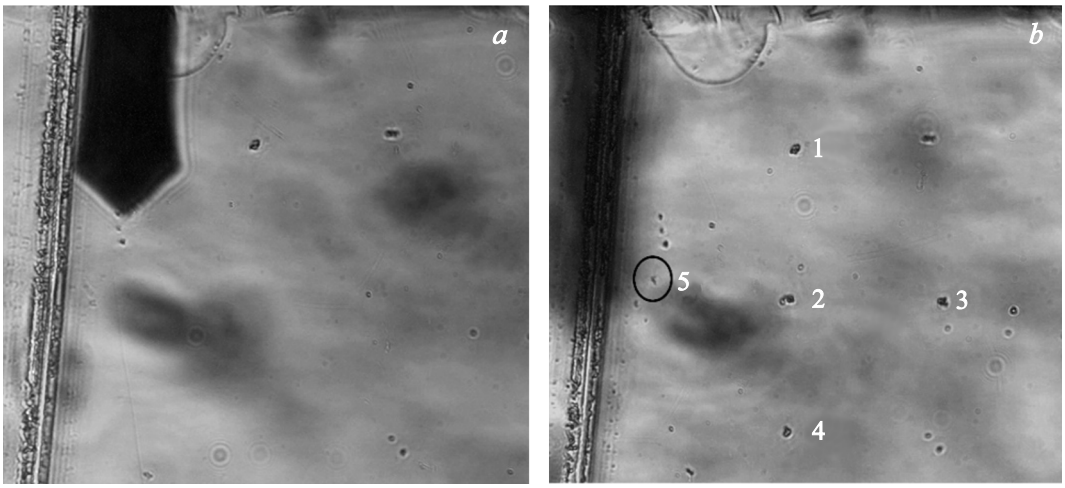

Figure 2. Optical images recorded during formation of the test structure in the form of a cross consisting of five upconversion particle agglomerates. Region with one particle (*a*), final image of the obtained structure (*b*). Numbers denote the particle deposition sequence, agglomerate 5 is marked with an oval for clarity.

image showed that this region contained a sufficient amount of upconversion particles that could be collected on the AFM probe for transferring onto another substrate. In this case, the AFM image contained a lot of noise („breaks“) that was likely induced by large difference in heights and interaction between the AFM probe and viscous solution residues.

Then, AFM was set to the contact mode (this is a mode where the probe doesn't induce vibrations and feedback loop keeps constant cantilever bending) and scanning of a sufficiently large area was started. Increasing probe pressure on the surface due to transition into the contact mode and a large scanning field made it possible to observe through the optical microscope how thinning of the film with upconversion particles took place in the scanning region and in some cases partial „sticking“ of this film to the AFM probe. Some parts of the film were pushed to the scanning field edge. Thus, the operator got the AFM probe coated with solution residues with upconversion particles that could be used to create the desired structures on a clean substrate. The amount of particles collected on the AFM probe could be changed by changing the scanning area.

Since it was difficult to control the amount of particles collected on the probe, the test structures were formed in two stages. At the first stage, all particles collected on the AFM probe were transferred into a preselected region on clean substrate № 2. The probe was brought to the surface, AFM was set to the semi-contact mode, cantilever vibration amplitude close to the maximum allowable amplitude was chosen and frequency adjustment was performed in a wide range of 0.05−2 MHz (with natural vibration frequency of the cantilever with the probe of about 0.15 MHz). Due to this, agglomerates collected on the AFM probe were transferred („shook off“) onto the substrate. Then, the optical microscope was used to select a single agglomerate with the desired dimensions and shape from these agglomerates. This agglomerate was again transferred to the AFM probe due to its scanning. In this case, adhesion of upconversion particles to the substrate surface was much lower than in the case of solution deposition. Therefore, a separate agglomerate could be also transferred to the AFM probe in the semi-contact mode. Besides visual monitoring of the transfer of the upconversion particle agglomerate using the optical microscope, monitoring was also performed by the change (reduction) in the cantilever resonance vibration frequency. After agglomerate deposition on the substrate surface, the resonance frequency returned to the initial value.

A single agglomerate from the AFM probe was deposited into a particular point on substrate № 2, and, thus, the desired test structure was gradually formed. Optical images illustrating the sequence of formation of the cross-shaped structure consisting of five agglomerate points are shown in Figure 2. These images also show a shadow of the cantilever and a microscratch that was used to find the place where the structure was formed on the substrate.

The size of the formed test structure was estimated using the AFM in the semi-contact mode. A new Tap150Al-G probe was used for such measurements. Since the adhesion force between the test structure and substrate was weak and there was a risk of agglomerate displacement from their current position or agglomerate transfer onto the AFM probe, then, to increase the adhesion, a 40 nm metal layer was deposited on the formed test structure after the confocal microscope measurements. Deposition was performed using the MultiProbe P (Omicron) ultrahigh-vacuum system by electron beam sputtering of a solid-state nickel target. Due to a large height of the particle agglomerate and convolution effect, the agglomerate's lateral dimensions observed through AFM could be much larger than the real ones. However, the convolution effect

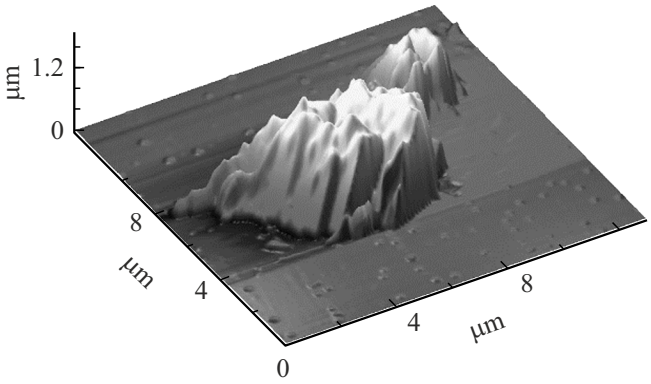

Figure 3. 3D AFM image of the particle agglomerate located in the center of the formed cross-shaped test structure.

doesn't affect the measurement of the structure height, and these dimensions were measured with accuracy of about 10 nm. Thee-dimensional image of one of the deposited agglomerates (central agglomerate in the structure) is shown in Figure 3. It can be clearly seen that the observed slope of the agglomerate side walls is defined by the AFM probe shape and, therefore, AFM images were not used to determine the lateral dimensions of the agglomerate.

1.5. Three-dimensional luminescent COM imaging of the sample

During scanning, an array of data was collected and represented a dependence of the luminescence intensity on the focal spot position. Scanning was performed in the (X, Y) plane perpendicular to the optical axis using a positioning system on the basis of the Thorlabs GVS012 galvanometric scanner, and over the sample depth Z (parallel to the optical axis) using the Newport NPO-140SG-D piezoscanner. Scanned surface area was 2.5×2.5 mm, depth scanning range was $100\,\mu$m. Scanning step in the test conditions was set to $3.25\,\mu$m in the(X, Y) plane and to $2\,\mu$m along the Z axis. Finally, a set of optical images was provided and represented an intensity distribution in the X and Y coordinates, with a step along the Z axis (see the schematic diagram in Figure 4). Hereinafter the $Z = 0$ coordinate corresponds to the substrate surface level, on which the test sample is placed.

It is important to note that the principle of detecting an optical signal from discrete light sources on the confocal microscope has a set of particular features. Suppose a point light source with the (X', Y') coordinates falls into the excitation beam focus (Figure 5, *a*). On the cross-section with the Z' coordinate, the maximum object luminescence intensity will correspond to this object. Any vertical deviation from $Z' + \delta z$ will lead to a decrease in the intensity. However, if the point light source is now placed near the excitation focal spot $(X' + \delta x, Y' + \delta y)$, then the intensity distribution pattern with vertical coordinate variation $Z' + \delta z$ will be fully changed: a local minimum will correspond to Z', and $Z' + \delta z$ will lead to the growth of the

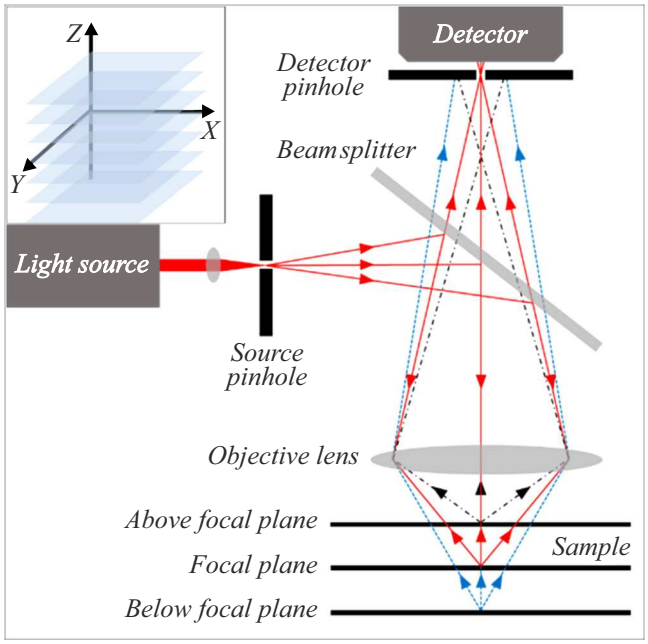

Figure 4. Schematic diagram of COM. Inset: diagram of 3D luminescent imaging of a bulk sample in the form of a set of flat cross-sections in the (X, Y) plane with a spep along the Z axis.

signal due to an increase in irradiation intensity (Figure 5, *b*). It should be generally expected that luminescence intensity distribution near point light source will have more than one pronounced maximum, which is the source of artefacts in the mathematical data analysis. The situation will get even more complicated, if the scanning Z axis is slightly inclined with respect to the optical axis (Figure 5, *c*). Such artefact may have a clearly pronounced maximum that, however, doesn't correspond to the true point light source position.

The next important point is the resolution of the resulting luminescent pattern Res that is defined by the microscope configuration. The objective parameters are evaluated using the Abbe equations as follows:

$$Res(x, y) = \lambda/(2 \cdot \eta \cdot \sin\alpha), \quad (1)$$

$$Res(z) = 2 \cdot \lambda/(\eta \cdot \sin(\alpha))^2, \quad (2)$$

where λ is the detected light wavelength, and $\eta \cdot \sin(\alpha)$ is the numerical aperture of the objective. Objective was chosen from considerations that the scanning region corresponds to typical dimensions of irregularities in the test sample. Therefore, a tenfold objective with a numerical aperture of 0.25 was used for measurements. According to Abbe criteria (1), (2), it provides the lateral resolution (in the (X, Y) plane) $\sim 1\,\mu$m, and axial resolution (along the Z axis) $\sim 20\,\mu$m. However, note that the COM resolution along the Z axis also depends on other factors, including the position and size of the pinhole in front of the detector. Theoretically, the pinhole can improve the axial resolution by multiple times [18]. However, it turns out to be difficult to determine the true COM resolution

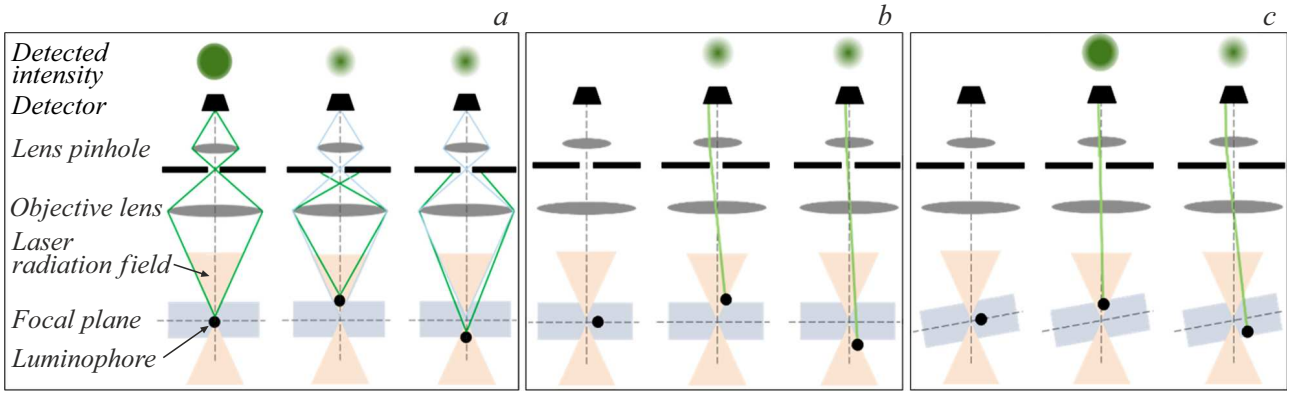

Figure 5. Diagram of luminescent imaging of discretely distributed luminescent objects for the cases when the object in the focal plane is within the excitation beam waist (*a*); the object in the focal plane is outside, but near the excitation beam (*b*); the sample with the object is placed at an angle to the excitation beam (*c*).

in practice. Therefore, it is necessary to achieve a 3D luminescent image that is adequate to the real distribution of discrete luminophores over the sample, and to determine the measurement error of the Z position of a point light source. It is important to add that the resulting COM resolution was intentionally „degraded“ by a sufficiently high lateral scanning step 3.25 μm to complicate functioning of the image recovery algorithms in the given test problem.

2. Findings and discussion

2.1. COM data array processing

Positions and dimensions of luminescent objects on the test structure surface were determined by mathematical processing of the data array consisting of the luminescent upconversion response intensity at 974 nm laser excitation, I_{XYZ}. X, Y, Z define the scanning region coordinates: X and Y are the surface coordinates, Z is the vertical position of the COM focal region.

2.2. Averaging procedure with a priori known parameters

For quick evaluation of the discrete distribution of upconversion particles on the substrate surface, it is sufficient to use a simple data array processing algorithm that proved effective for the case of continuous distribution of luminophores [19]. A priori known upconversion particle layout on the surface makes it possible to determine the noise signal intensity in regions that don't contain upconversion luminescence sources I_0. Then, the height $H_{XY} = Z = 0\,\mu$m corresponding to the substrate surface level is assigned to all scanning regions, for which the signal level turns out to be below the threshold $I_{XYZ} < I_0$.

In the relevant regions $I_{XYZ} > I_0$ containing the luminescence sources, position of H_{XY} is determined as follows:

$$H_{XY} = \frac{\Sigma_Z Z \cdot I_{XYZ}^{\alpha}}{\Sigma_Z I_{XYZ}}. \qquad (3)$$

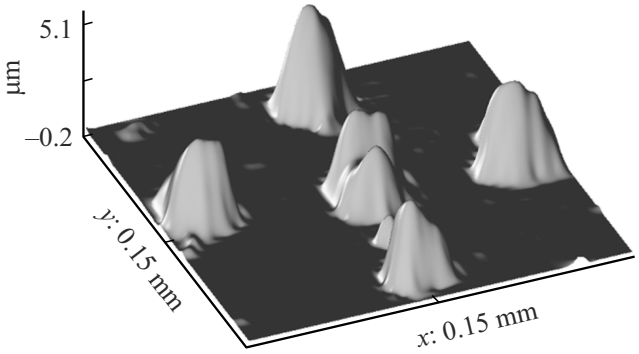

Figure 6. Upconversion luminophore agglomerate distribution in the test structure determined using the averaging procedure with a priori known parameter.

The power parameter α is introduced to control the contrast of the signal being analyzed. For example, in our case, the relative dispersion of luminescence intensity values in the relevant regions was equal to 4 orders. To reduce the contrast, α was set to $\alpha = 0.3$. To remove high-frequency noise, average „smoothing“ may be carried out in the given region:

$$\overline{H}_{X_i,Y_j} = \frac{1}{(2k+1)^2} \sum_{i-k}^{i+k} \sum_{j-k}^{j+k} I_{X_i,Y_j}. \qquad (4)$$

For $k = 1$, the data processing result is shown in Figure 6. It can be seen that such simple approach generally determines luminescent object positions quite accurately. Whilst the information concerning the lateral dimensions and heights is not consistent with the reality. For example, particle 3 with dimensions $1.4 \times 1.1\,\mu$m (Table 1) in the recovered picture (Figure 6) spreads over the $10 - 15\,\mu$m region. According to Figure 6, object height determination accuracy may be estimated as 5 μm.

Table 1. Particle sizes measured using COM before and after the deconvolution procedure, and comparison with real sizes of the test structure

№ Particle	Dimension		
	X, μm	Y, μm	Z, μm
Without the deconvolution procedure, $r^{(a)}$			
1	6.0	4.0	15.4
2	6.9	6.5	21.3
3	6.5	5.6	22.7
4	7.0	4.6	16.6
5	6.9	5.5	19.9
After the deconvolution procedure, $r^{(b)}$			
1	3.9	3.4	2.0
2	5.6	3.3	3.5
3	3.3	3.3	2.8
4	5.5	3.6	1.8
5	3.3	3.2	2.0
True dimensions, $r^{(0)}$			
1	0.9	2.2	0.79
2	2.4	1.1	1.18
3	1.4	1.1	1.44
4	2.0	2.5	2.51
5	1.8	1.8	1.86

2.3. Deconvolution procedure on the basis of the point spread function

A more precise analysis of the experimental data array is based on deconvolution of the recorded 3D image using the Richardson-Lucy algorithm [20–23]. This method describes a confocal microscopy image using the following model:

$$g(X,Y,Z) = (f(X,Y,Z) \otimes p(X,Y,Z)) + n(X,Y,Z), \quad (5)$$

where f is the initial (ideal) image, p is the point spread function (PSF), n — is the additive noise, $\otimes$ is the convolution operation. Since the convolution operation in a spatial region is equivalent to the element-by-element multiplication in the Fourier space, it is convenient to transfer all calculations into the Fourier space:

$$G(S_x,S_y,S_z) = F(S_x,S_y,S_z) \cdot P(S_x,S_y,S_z) + N(S_x,S_y,S_z), \quad (6)$$

where G, F, P and N are Fourier transforms of g, f, p and n, respectively, (S_x,S_y,S_z) are Fourier domain coordinates. As can be seen from equation (6), data on $P(S_x,S_y,S_z)$ is insufficient for accurate recovery of the initial image $F(S_x,S_y,S_z)$ due to the contribution of an unknown noise component N. An attempt to perform deconvolution (division in the Fourier domain) results in uncertainty in those regions where $P(S_x,S_y,S_z)$ are close to zero.

Noise effect on the image recovery may be minimized using an iterative deconvolution method — Richardson-Lucy algorithm (RL algorithm) that is mathematically formulated as follows:

$$\tilde{f}_{k+1} = \tilde{f}_k \left(\frac{g}{\tilde{f}_{k \otimes p} \otimes \hat{p}} \right), \quad (7)$$

where $\tilde{f}_k$ is the recovered image at the k-th iteration, $\hat{p}$ is the transposed PSF matrix defined as $\hat{p}(X,Y,Z) = p(-X,-Y,-Z)$. RL algorithm has convergence, i.e. with $k \to \infty$, the recovered image tends to the true one. However, accurate recovery is impossible in practice due to inaccurate value of PSF and the presence of noise n that distorts the data.

To determine PSF, we performed 3D scanning of a luminescent signal that was the smallest among luminescent objects that were sufficiently bright for detection. Signal-to-noise ratio was approximately 10^4, which allowed the noise component to be neglected in equation (6). Thus, $p(X,Y,Z)$ calculated using $P(S_x,S_y,S_z) = G(S_x,S_y,S_z)/F(S_x,S_y,S_z)$ and inverse Fourier transform takes a form shown in Figure 7. Using the obtained PSF and RL algorithm on the basis of iterative equation (7), 3D distribution of luminescent objects on the test structure was obtained (Figure 8).

True heights of luminescent objects were determined using the AFM data (dimension Z). As mentioned above, to determine lateral dimensions using the AFM method, dimensions of the probe used for scanning and

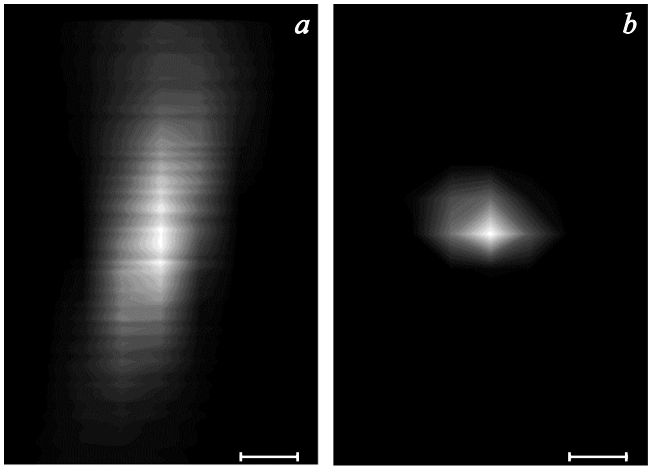

Figure 7. $p(X,Y,Z)$ projection on the XZ plane (a) and the XY plane (b). The function was calculated using the results of COM scanning data processing for single luminophore upconversion luminescence. Scale bar size is $5\,\mu$m. Shades of grey are proportional to the point spread function amplitude.

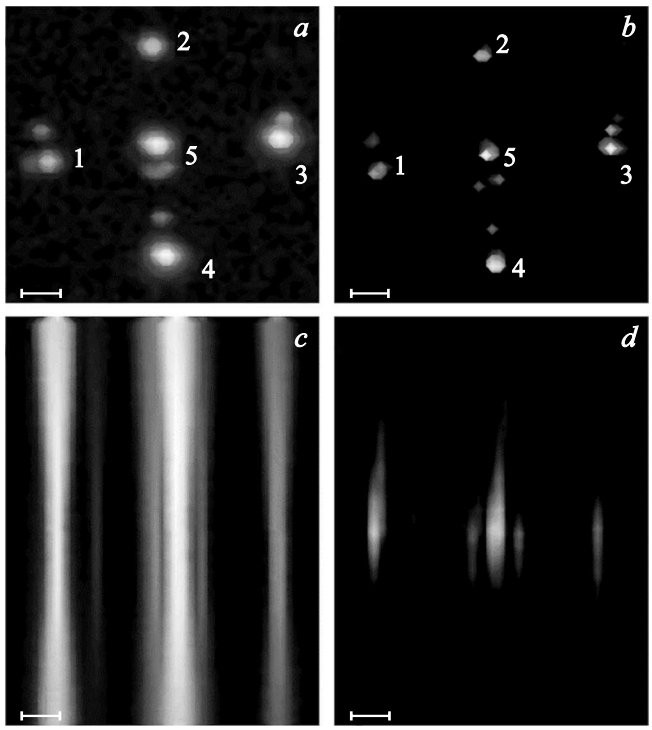

Figure 8. $I_{X,Y,Z}$ projections (3D scanning of test structure luminescence intensity scanning) on the XY plane (a) and the XZ plane (c). $f_{X,Y,Z}$ test structure image (obtained using the deconvolution procedure) projection on the XY plane (b) and the XZ plane (d). Bar size is $20\,\mu$m. Shades of grey are proportional to the relative amplitudes of $I_{X,Y,Z}$ and $f_{X,Y,Z}$.

Table 2. Luminescent object dimension measurement errors

ΔX, μm	ΔY, μm	ΔZ, μm
Without the deconvolution procedure, $\Delta r^{(a)}$		
6.6	5.3	23.1
With the deconvolution procedure, $\Delta r^{(b)}$		
3.9	2.7	2.4
Resolution improvement, $\Delta r^{(a)}/\Delta r^{(b)}$		
$\Delta x^{(a)}/\Delta x^{(b)}$	$\Delta y^{(a)}/\Delta y^{(b)}$	$\Delta z^{(a)}/\Delta z^{(b)}$
1.7	1.9	9.6

the deconvolution procedure shall be considered. Therefore, COM with $40\times$ objective and a resolution of $\sim 0.4\,\mu$m (dimension X, Y) was used to determine true lateral dimensions of luminescent objects. Data in Table 1 are used to evaluate the dimension measurement errors for the numbered luminescent objects listed in Table 2. It can be seen from the table that the deconvolution procedure improves the lateral resolution by 2 times, and the axial resolution along the Z axis almost by 10 times.

Conclusion

It is known that simple mathematical processing methods based on finding the maximum signals with subsequent high-frequency noise filtration give good results for continuous luminophore distribution over the given object surface [19]. Investigations of the luminescent tomography of a test structure with a predefined pronounced discrete distribution of upconversion $NaYF_4$:Yb, Er particle agglomerates have shown that this technique was unsuitable for true image recovery even when the noise level was known. According to Figure 6, such approach may be used to evaluate only luminescent particle agglomerate locations. Whilst the information concerning the lateral dimensions and heights is not consistent with the actual ones. For luminescent tomography of discrete media, it is essential to consider deconvolution during image recovery. For this, the point spread function shall be known. This function may be obtained by means of 3D scanning of luminescence intensity from a pseudo-point single luminophore whose dimensions are smaller than the lateral resolution of the objective used in the experiment. In this case, the convolution procedure with the RL algorithm becomes applicable. Experiments with the test structure have shown that this data processing method has improved the lateral resolution by two times and axial resolution by an order of magnitude, which was finally $\sim 3-4\,\mu$m. Considering the mean biological cell size approximately equal to $10-50\,\mu$m, it can be seen that the obtained resolution is sufficient for luminescent tomography of the intracellular distribution of upconversion bioprobes.

Acknowledgments

Synthesis of upconversion nanoparticles was supported by Grant № 23-42-10012 provided by the Russian Science Foundation (https://rscf.ru/project/23-42-10012/); spectroscopic and AFM investigations were performed for a topic within the state assignment of the Federal Research Center — Kazan Scientific Center of the Russian Academy of Sciences.

Experiment data postprocessing performed by D.G.Zverev and P.A.Kosach was supported by the subsidy provided to Kazan Federal University to fulfil a state research assignment (project FZSM-2024-0010).

Conflict of interest

The authors declare no conflict of interest.

References

[1] D. Huang, E.A. Swanson, C.P. Lin, J.S. Schuman, W.G. Stinson, W. Chang, M.R. Hee, T. Flotte, K. Gregory, C.A. Puliafito, J.G. Fujimoto. Science, **254**, 1178 (1991). DOI: 10.1126/science.1957169

[2] S.W. Paddock. Bio Techniques, **27** (5), 992 (1999). DOI: 10.2144/99275ov01

[3] K. Shi, P. Li, S. Yin, Z. Liu. Optics Express, **12** (10), 2096 (2004). DOI: 10.1364/OPEX.12.002096
[4] B. Rosal, D. Jaque. Methods Appl. Fluorescence, **7** (2), 022001 (2019). DOI: 10.1088/2050-6120/ab029f
[5] H. Li, M. Tan, X. Wang, F. Li, Y. Zhang, L. Zhao, C. Yang, G. Chen. J. American Chem. Society, **142** (4), 2023 (2020). DOI: 10.1021/jacs.9b11641
[6] W. Jiang, J. Yi, X. Li, F. He, N. Niu, L. Chen. Biosensors, **12**, 1036 (2022). DOI: 10.3390/bios12111036
[7] G. Lee, Y.I. Park. Nanomaterials, **8** (7), 511 (2018). DOI: 10.3390/nano8070511
[8] H. Lv, J. Liu, Y. Wang, X. Xia, Y. Li, W. Hou, F. Li, L. Guo, X. Li. Frontiers in Chemistry, **10**, 996264 (2022). DOI: 10.3389/fchem.2022.996264
[9] Y. Han, Y. An, G. Jia, X. Wang, C. He, Y. Ding, Q. Tang. Nanoscale, **10**, 6511 (2018). DOI: 10.1039/C7NR09717D
[10] G. Ren, S. Zeng, J. Hao. J. Phys. Chem. C, **115**, 20141 (2011). DOI: 10.1021/jp2064529
[11] E.O. Mityushkin, D.K. Zharkov, A.V. Leontiev, L.A. Nurtdinova, A.G. Shmelev, V.G. Nikiforov. Izvestiya RAN. Ser. fiz., **87** (12), 310 (2023) (in Russian). DOI: 10.31857/S0367676523702976
[12] D.K. Zharkov, O.E. Mityushkin, A.V. Leontiev, L.A. Nurtdinova, A.G. Shmelev, N.M. Lyadov, A.V. Pashkevich, A.P. Saiko, O.Kh. Khasanov, V.G. Nikiforov. Izvestiya RAN. Ser. fiz., **87** (12), 310 (2023) (in Russian). DOI: 10.31857/S036767652370299X
[13] A.D. Elliott. Current Protocols in Cytometry, **92** (1), e68 (2019). DOI: 10.1002/cpcy.68
[14] R.H. Webb. Rep. Prog. Phys., **59** (3), 427 (1996). DOI: 10.1088/0034-4885/59/3/003
[15] J.M. Binder, A. Stark, N. Tomek, J. Scheuer, F. Frank, K.D. Jahnke, C. Müller, S. Schmitt, M.H. Metsch, T. Unden, T. Gehring, A. Huck, U.L. Andersen, L.J. Rogers, F. Jelezko. SoftwareX, **6**, 85 (2017). DOI: 10.1016/j.softx.2017.02.001
[16] A.P. Tchuklanov, A.S. Morozova, N.I. Nurgazizov, E.O. Mityushkin, D.K. Zharkov, A.V. Leontiev, V.G. Nikiforov. ZhTF, **93** (7), 1019 (2023) (in Russian). DOI: 10.21883/JTF.2023.07.55763.82-23
[17] A.P. Chuklanov, A.S. Morozova, Ye.O. Mityushkin, A.V. Leontyev, L.A. Nurtdinova, V.G. Nikiforov, N.I. Nurgagizov Bull. Russ. Academy Sciences: Physics, **88** (12), 1971 (2024). DOI: 10.1134/S1062873824708559
[18] T. Wilson. J. Microscopy, **244**, 113 (2011). DOI: 10.1111/j.1365-2818.2011.03549.x
[19] A.V. Leontiev, L.A. Nurtdinova, E.O. Mityushkin, A.G. Shmelev, D.K. Zharkov, V.V. Andrianov, L.N. Muranova, Kh.L. Gainutdinnov, R.R. Zairov, A.R. Khazieva, A.R. Mustafina, V.G. Nikiforov. ZhTF, **94** (9), 1576 (2024) (in Russian). DOI: 10.61011/JTF.2024.09.58680.83-24
[20] W.H. Richardson. J. Opt. Soc. Am., **62**, 55 (1972). DOI: 10.1364/JOSA.62.000055
[21] L.B. Lucy. Astronom. J. **79**, 745 (1974). DOI: 10.1086/111605
[22] N. Dey, L. Blanc-Feraud, C. Zimmer, Z. Kam, J.-C. Olivo-Marin, J. Zerubia. 2004 2nd IEEE Intern. Sympos. Biomed. Imaging: Nano to Macro (IEEE Cat No. 04EX821) (Arlington, VA, USA, 2004), v. 2, p. 1223–1226, DOI: 10.1109/ISBI.2004.1398765
[23] P.J. Shaw. *Comparison of Widefield/Deconvolution and Confocal Microscopy for Three-Dimensional Imaging* in: J. Pawley (eds) Handbook Of Biological Confocal Microscopy (Springer, Boston, MA. Handbook of Biological Confocal Microscopy, Third Edition, edited by J.B. Pawley, (Springer, Boston, MA, 2006)), DOI: 10.1007/978-0-387-45524-2_23

Translated by E.Ilinskaya